Field investigation and model tests on differential settlement of houses due to liquefaction in the Niigata-ken Chuetsu-Oki Earthquake of 2007

K. Isobe & S. Ohtsuka
Nagaoka University of Technology, Japan

H. Nunokawa
Central Japan Railway Company, Japan

SUMMARY
A massive earthquake struck the Niigata Chuetsu-Oki region of Japan on July 16th, 2007, claiming 11 lives and damaging about 1,000 houses. The tremor had a magnitude of 6.8, with data from an accelerograph managed by a nationwide strong-motion observation network known as Kyoshin Net (K-net) showing a maximum value of 680 gal. In the Matsunami district (located on land filled and developed as a residential area from around 1970 onward) about 3 km northeast of Kashiwazaki Station, many houses were damaged due to liquefaction. Field investigation, including a boring survey, surface wave exploration and measurement of differential settlement of houses knocked aslant by soil liquefaction, was conducted to determine the relationship between the extent of damage to houses and the area's geological structure. It was found that most houses severely damaged due to liquefaction were located around the boundary between sand dunes and the local river delta. Additionally, the relationships linking sloping geological structure, the thickness of the liquefaction layer and total/differential settlement of houses were clarified from the results of shaking table model tests conducted in this study.

Keywords: liquefaction, differential settlement, shaking table tests, triaxial test, surface wave exploration

1. INSTRUCTIONS

The Niigata-ken Chuetsu-Oki Earthquake that hit Japan on July 16th, 2007, killed 11 people and damaged more than 1,000 houses. The quake registered 6.8 on the magnitude scale of the Japan Meteorological Agency (JMA), and a K-net accelerograph measured a maximum value of 680 gal. Many houses were damaged, and ground deformation types such as liquefaction were observed in Kashiwazaki City and Kariwa Village (Figure 1.1 (a)). In the Hashiba district of Kashiwazaki City and in Kariwa Village, foundation damage to wooden houses and ground deformation were extensively observed. In these areas, liquefaction-related damage to houses and ground failure similar to those

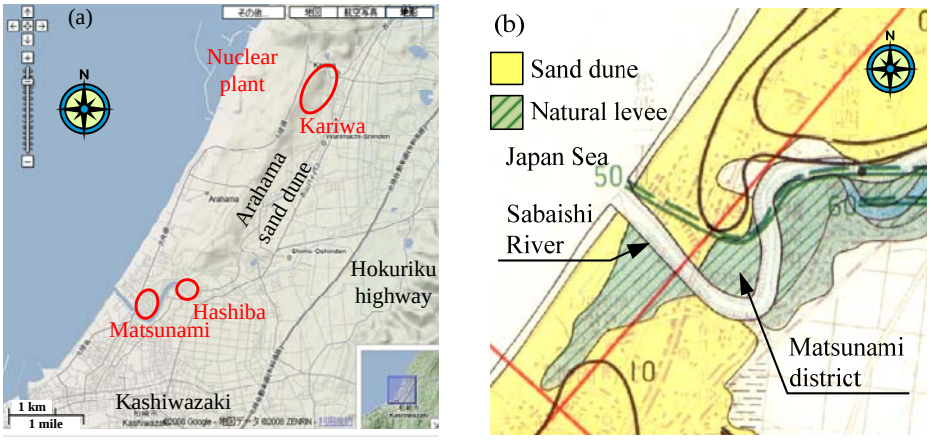

Figure 1.1. (a) Liquefaction site in Kashiwazaki and Kariwa in the Niigata-ken Chuetsu-Oki Earthquake of 2007 (map by Google map) and (b) Terrain classification map around Matsunami district

seen in the Mid Niigata Prefecture Earthquake of 2004 also occurred. This was the second experience of severe earthquake damage in the region within a span of three years.

This paper reports on the results of earthquake damage investigation work conducted in the Matsunami district of the region. The relationship between ground conditions and the characteristics of damage to houses was investigated based on the outcomes of surface wave exploration, Swedish weight sounding (SWS) tests, boring investigation involving standard penetration tests (SPT) and measurement of differential settlement in damaged houses. The relationships linking sloping geological structure, the thickness of the liquefaction layer and total/differential settlement of houses were also discussed based on the results of shaking table model tests.

2. FIELD INVESTIGATION

2.1. Overview of geographical conditions in Kashiwazaki City

The Matsunami district sits on land filled for the development of a residential area from around 40 years ago. It is located about 3 km northeast of Kashiwazaki Station on the right bank of the Sabaishi River near its mouth and on the hinterland of the Arahama dunes. According to the terrain classification map for the district (Figure 1.1 (b)), the northwestern part of Matsunami is classified as sand dunes, and the southeastern part is a natural levee area.

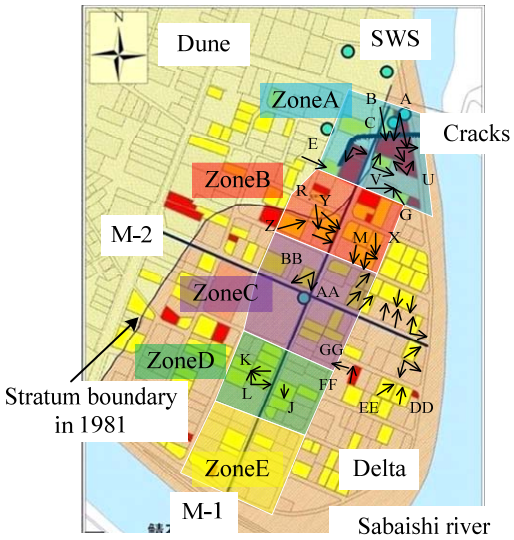

Figure 2.1. Distribution of damaged houses and ground investigation sites in Matsunami

2.2. Overview of damage caused by the earthquake

Figure 2.1 shows the distribution of damaged houses in Matsunami based on the emergency risk judgment table for residential structures. Here, yellow areas show a warning level (corresponding to light damage), red areas show a dangerous level (corresponding to severe damage), and the arrows on the houses indicate the direction of inclination resulting from the damage. The stratum boundary in the figure is the border between the sand dune and delta (natural levee) areas based on Figure 1.1 (b). Table 2.1 shows the maximum differential settlement and maximum tilt angle of damaged houses as calculated from the foundation height at their corners and the distance between the measurement points. Figure 2.2 shows the results of analysis on differential settlement and tilt angle by zone.

Damaged houses with red marks are distributed in zones A and B along the stratum boundary, while yellow-marked houses are distributed extensively. The maximum tilt angle observed in most houses was beyond the acceptable limit (4/1000) specified in Recommendations for the Design of Small

Building Foundations (2008). The most severely damaged structures stood on the stratum boundary located in the northern part of Matsunami, where ground cracks were observed (figures 2.3 (a) and (b)). The maximum differential settlement in the area was more than 200 mm (in the location of the shaded houses in Table 2.1). Signs of liquefaction such as sand boiling were observed in central and eastern areas of the district such as zones C and D (Figure 2.3 (c)). However, differential settlement of damaged houses in these areas was less prominent than that of structures in the northern area. The reasons for this are highlighted by the results of the ground investigation as outlined below.

Table 2.1. Maximum differential settlement and maximum tilted angle measured in Matsunami

Zone	Symbol	Maximum differential settlement [mm]	Maximum tilted angle	Zone	Symbol	Maximum differential settlement [mm]	Maximum tilted angle
A	A	678	20/1000	C	O	79	7/1000
	B	403	23/1000		P	33	3/1000
	C	222	22/1000		AA	106	16/1000
	W	104	14/1000		BB	91	9/1000
	U	220	54/1000		S	141	15/1000
	V	215	25/1000		I	117	9/1000
	E	8	1/1000		H	50	5/1000
	F	87	6/1000		T	49	8/1000
	G	42	4/1000		CC	168	39/1000
B	R	84	6/1000	D	DD	68	11/1000
	X	68	12/1000		EE	67	8/1000
	Y	283	25/1000		FF	127	17/1000
	Z	91	10/1000		GG	34	12/1000
	M	127	6/1000		J	127	17/1000
	N	158	24/1000		K	98	7/1000
	Q	136	12/1000		L	58	5/1000

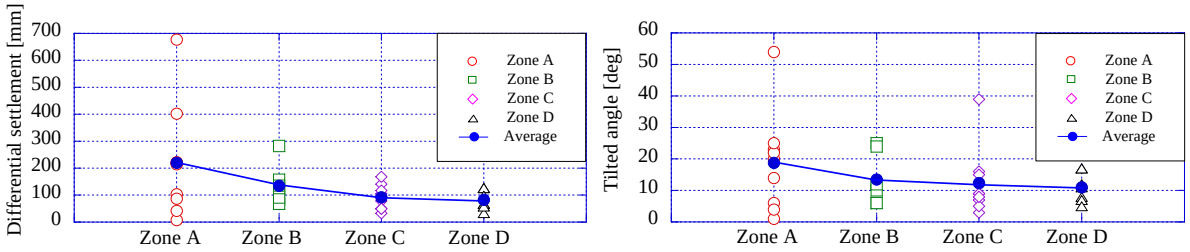

Figure 2.2. Differential settlement and tilted angle of houses observed in Matsunami residential district

Figure 2.3. Earthquake damage in Matsunami district; (a) the severest damaged house, (b) damaged houses due to ground crack and (c) signs of liquefaction (sand boiling)

2.3. Results of surface wave exploration

To investigate ground conditions, surface wave exploration was conducted on the lines shown in Figure 2.1, where M-1 and M-2 indicate the north-south line and the east-west line, respectively. SWS

and boring surveys were also executed at the position of the circle in the figure. The results of these tests are shown in Figure 2.4. The groundwater level in the area was estimated to be about 2 m to 3 m below the ground surface. A slightly loose sand layer with a shear wave velocity of 120 – 150 m/s was located below the surface to a depth of 5 m, and a dense sand layer with a shear wave velocity of 150 – 200 m/s was present beneath this. The S-velocity distribution corresponded to the specifications of the 1981 geographic map. The worst-hit damage zone was on the stratum boundary between the sand dune and delta areas, and the dense sand layer inclined significantly toward the delta area in the zone.

Figure 2.5 shows the results of simple liquefaction judgment such as FL (factor of liquefaction) and PL (potential liquefaction) values calculated using the shear wave velocity on the M-1 line according to reference literature (Andrus et al., 1999; Japan Road Association; 2002). These results indicate that the FL value in the delta area with its loose sand layer was less than 1.0, while the corresponding value in the sand dune area with its dense sand layer was over 1.0. The PL value changed rapidly along the stratum boundary between the sand dune and delta areas. This is considered to be why the severest differential settlement of houses around the stratum boundary was seen in the Matsunami district.

The following conclusions were drawn from the investigation in the Matsunami district:
1) The severest damage to houses was seen around the stratum boundary between the sand dune area and the delta of the Sabaishi River.
2) Although signs of liquefaction such as sand boiling were observed in the delta area, the maximum differential settlement and inclination angle of houses were smaller than those around the boundary.
3) This was because the sand dune layer inclined toward the delta, and ground cracks occurred due to lateral flowing of the surface ground.

3. SHAKING TABLE MODEL TESTS

3.1. Physical properties and mechanical characteristics of soil used in the model tests

3.1.1. Material and testing procedure

Kariwa sand samples from Kariwa Village near Kashiwazaki City were used to represent liquefied ground material in the model tests. Tohoku silica sand #6 was also used as non-liquefied ground material. The Kariwa sand was washed and passed through a 2 mm sieve, producing a mass of particles with diameters in the range from 2 mm to 75 μm. The physical properties of both sand types are shown in tables 3.1 through 3.3. The maximum and minimum void ratios of both types were measured using the Japanese standard method. Figure 3.1 shows the grain size accumulation curve for sand samples from Kariwa and Matsunami. As their physical characteristics are similar, Kariwa sand was used to represent liquefied ground material in the tests.

Static and cyclic CU tri-axial tests were carried out to clarify the mechanical characteristics and liquefaction strength of Kariwa sand. Two specimens were created for the tests as follows: (1) an undisturbed specimen sampled from the Inaba district of Kariwa Village using the freezing sampling method, and (2) a reconstituted specimen molded with an initial relative density identical to that of the undisturbed sample (Dr = 40%) made from a sample used in the above tests by pluviating air-dried particles through air. Pluviation apparatus was set up so that while the particles fell into the mold, the sand container was moved upward to maintain a constant drop height between the container and the mold. The specimens were molded into dimensions of 5 cm in diameter 10 cm in height. Tables 3.4 and 3.5 show the static and cyclic CU tri-axial tests, respectively.

The test apparatus consisted of a triaxial cell, cell-pressure and back-pressure control devices, an axial load control device and a data acquisition/recording system to collect data on the axial load, axial displacement and pore water pressure of the specimens and on volume reduction during consolidation (i.e., water drainage from the specimens). After a self-sustaining sample had been obtained by applying a 20 kPa vacuum to the sample interior, a cylindrical chamber and cell cover were set up, and the cell was filled with water. To achieve a high degree of saturation, vacuum conditions were applied to both the cell and the sample interior in such a way that the confining stress was constant (20 kPa)

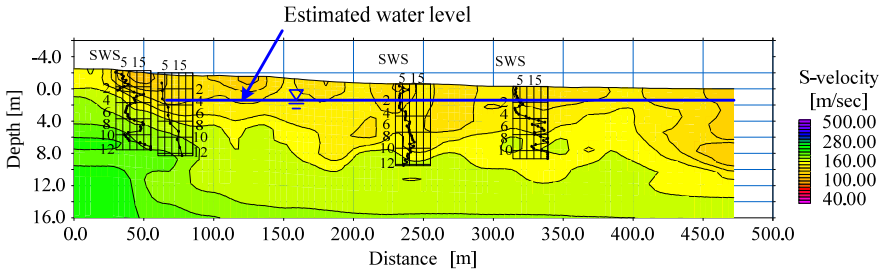

Figure 2.4. Ground investigation results (Surface wave search, SWS, boring investigation) in M-1 line

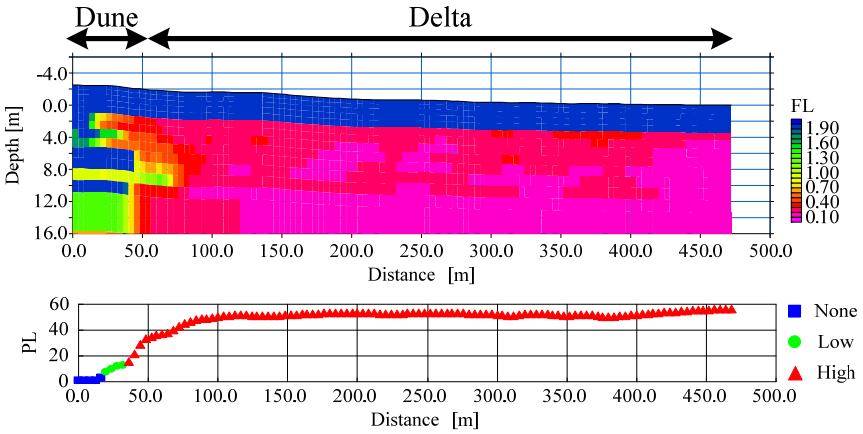

Figure 2.5. Simple liquefaction judgments using surface wave results in Matsunami (M-1 line)

during the process. After the final stage of this process was reached (-80 kPa for cell pressure and -100 kPa for the interior sample), deaerated water was circulated into the specimen for about 2 hours, and the pressure of the sample interior and the cell were returned to -20 kPa and 0 kPa, respectively. The back pressure was then increased gradually to 100 kPa, and pressure of 150 kPa was simultaneously applied to the cell so that the confining stress was held constant at 50 kPa. To ensure specimen saturation, the degree of saturation was evaluated at this stage based on the *B*-value, defined as the ratio of the pore water pressure increment to the isotropic stress increment under undrained conditions. Using this procedure, the test was continued until the *B*-value of the specimen was equal to or greater than 0.95. The specimen was consolidated isotropically for 6 hours under a confining pressure of 50 – 300 kPa. In order to examine static shear strength and liquefaction strength, static and cyclic tests were performed by applying deviator stress at a loading rate of 0.05 mm/min and uniform sinusoidal cycles of deviator stress at a frequency of 0.01 Hz with a varying cyclic stress ratio under constant cell pressure. Axial loads were measured using a load cell with a capacity of 5 kN installed between the top cap of the pedestal and the piston in the cell, and axial strain was monitored using a displacement transducer outside the cell. The electrical outputs collected from the load cell, the displacement transducer, the pore water pressure transducer and the gap sensor for the measurement of specimen volume reduction during consolidation were amplified and recorded simultaneously using a computer.

3.1.2. Results

Figures 3.2 (a) and (b) show the effective stress paths of the static CU tri-axial tests for both samples. It can be seen that the angles of shear resistance ϕ' for the undisturbed and reconstituted samples were 35.9 and 34.6 degrees, respectively. These figures indicate typical undrained cyclic behavior of regular loose sand; that is, pore water pressure rises with increasing strain before deviator stress approaches the failure line, and volume expansion is seen after its approach.

Figures 3.3 (a) and (b) show the effective stress paths of the cyclic CU tri-axial tests for both samples, and illustrate typical undrained cyclic behavior of regular sand; that is, pore water pressure gradually rises with cyclic loading, and shear strain increases dramatically when cyclic loading is generated near

Table 3.1. Soil physical property of Kariwa sand

Maximum dry density ρ_{dmax} [g/cm^3]	1.712	Maximum grain size	0.85
Minimum dry density ρ_{dmin} [g/cm^3]	1.424	D_{60}	0.35
Soil particle density ρ_s [g/cm^3]	2.742	Mean grain size D_{50}	0.34
Maximum void ratio e_{max}	0.926	D_{30}	0.30
Minimum void ratio e_{min}	0.602	D_{10}	0.15
Coefficient of permeability [cm/s]	2.80 x 10^{-2}	Uniformity coefficient U_c	2.33
		Coefficient of curvature U_c'	1.71

Table 3.2. Soil physical property of Tohoku silica sand #6

Maximum dry density ρ_{dmax} [g/cm^3]	1.695	Maximum grain size	0.85
Minimum dry density ρ_{dmin} [g/cm^3]	1.401	D_{60}	0.35
Soil particle density ρ_s [g/cm^3]	2.630	Mean grain size D_{50}	0.34
Maximum void ratio e_{max}	0.878	D_{30}	0.30
Minimum void ratio e_{min}	0.551	D_{10}	0.23
Coefficient of permeability [cm/s]	-	Uniformity coefficient U_c	1.52
		Coefficient of curvature U_c'	1.12

Table 3.3. Soil physical property in Matsunami district

Stratum type		Sandy soil As1	New dune Asd	Old dune Dsd
Grain size distribution	Gravel [%]	0 ~ 17	0 ~ 1	0
	Sand [%]	71 ~ 93	85 ~ 99	89 ~ 96
	Fines [%]	5 ~ 29	1 ~ 9	4 ~ 11
Uniformity coefficient U_c		2.56 ~ 4.35	1.86 ~ 3.69	2.06 ~ 2.46
Mean grain size D_{50}		0.26 ~ 0.59	0.29 ~ 0.49	0.27 ~ 0.33

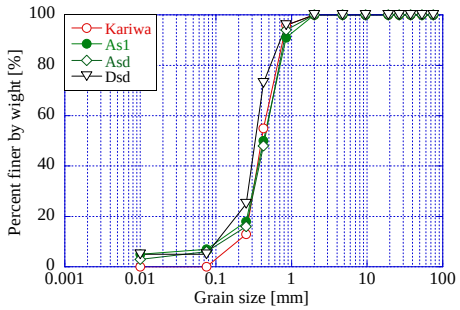

Figure 3.1. Grain size accumulation curve of soil sampled in Kariwa and Matsunami

Table 3.4. Static tri-axial compression test cases

Name of sample	Void ratio e	Effective confining pressure [kPa]	Back pressure [kPa]	Loading speed [% / min]
Undisturbed sample	0.876 – 0.889	50, 75, 100	100	0.05
Reconstitution sample	0.796	100, 200, 300	100	0.05

Table 3.5. Cyclic tri-axial compression test cases

Name of sample	Void ratio e	Effective confining pressure [kPa]	Back pressure [kPa]	Frequency [Hz]	$\sigma_d / 2\sigma'_0$
Undisturbed sample	0.770 – 0.813	100	100	0.1	0.124
					0.179
					0.219
					0.275
Reconstitution sample	0.796	100	100	0.1	0.141
					0.175
					0.205
					0.241
					0.324

the failure line. Cyclic mobility occurs as the stress path cycles through a zero-effective confining pressure. As shown in these figures, both curves reach a steady state with generation of cyclic mobility as per the common behavior of regular sand. Figures 3.4 (a) and (b) show the relationships between the cyclic stress ratio $\sigma_d / 2\sigma'_0$ and the number of cycles N_c causing liquefaction, defined as a strain double amplitude DA of 5% for both samples. From the results, the liquefaction strengths for the undisturbed sample and the reconstituted sample are defined as 0.191 and 0.166, respectively. It was thus understood that Kariwa sand is easily liquefied.

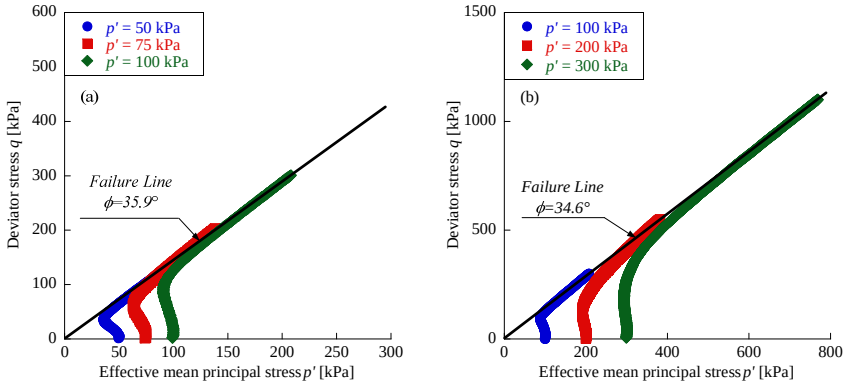

Figure 3.2. Effective stress paths of (a) undisturbed and (b) reconstitution sample under static monotonic loading

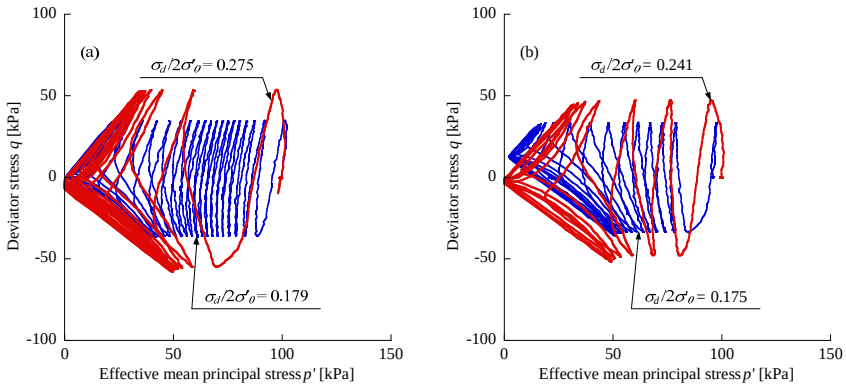

Figure 3.3. Effective stress paths of (a) undisturbed and (b) reconstitution sample under cyclic loading

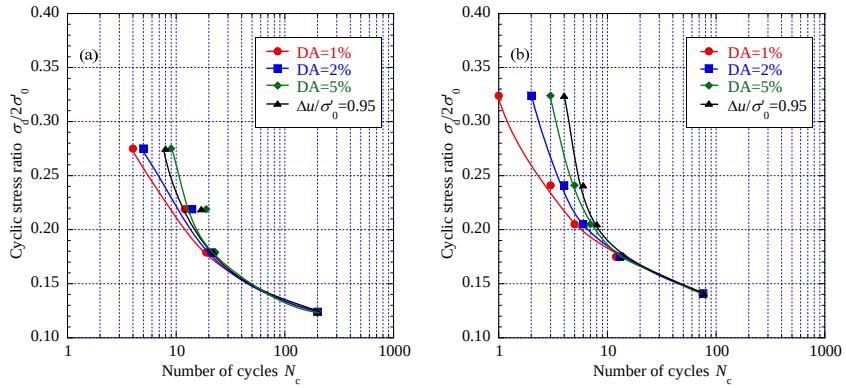

Figure 3.4. Liquefaction strength curves of (a) undisturbed and (b) reconstitution sample of Kariwa sand

3.2. Overview of the model tests

Based on the above observations in the field, shaking table model tests under 1 G gravity conditions were conducted to investigate the relationships linking sloping geological structure, the thickness of

the liquefaction layer and total/differential settlement of houses. Figure 3.5 shows a sectional side view of the model tests. The soil chamber, which measured 300 mm in length, 1,100 mm in width and 400 mm in depth, had water tanks on its left and right sides to supply the model ground with water. Cushioning material was attached to the sidewall surface in order to reduce the influence of reflected wave during shaking. The specifications of the model ground were based on the results of surface wave exploration conducted at the M-1 line in consideration of the similarity ratio. The thicknesses of the liquefied and non-liquefied layers were 200 mm and 100 mm, respectively, and the angle of the slope was 1:1.5 as shown in Figure 3.7. The liquefied layer was modeled by pluviating air-dried particles through water using Kariwa sand with a relative density of 40%, and the non-liquefied layer was modeled via the tamping method using Tohoku silica sand #6 with a relative density of 100%.

The positions of the foundation model were varied from [1] to [5] as shown in Figure 3.5 to survey the influence of liquefied layer thickness imbalance under the foundation. Table 3.6 shows the test cases, the relative density and the thickness of the liquefied layers unbalanced under the model foundation of each case before shaking. Figure 3.6 shows the location of measurement sites for variables such as acceleration, displacement and pore water pressure. As input, 40 cycles of an 8 Hz sinusoidal wave with a slope were used. The target acceleration was 250 gal. Considering the similarity ratio, the weights of the 150 mm x 150 mm square foundation model and the ground contact pressure were set to 7.8 x 10^{-3} kN and 0.34 kPa, respectively. The data sampling frequency was 1000 Hz.

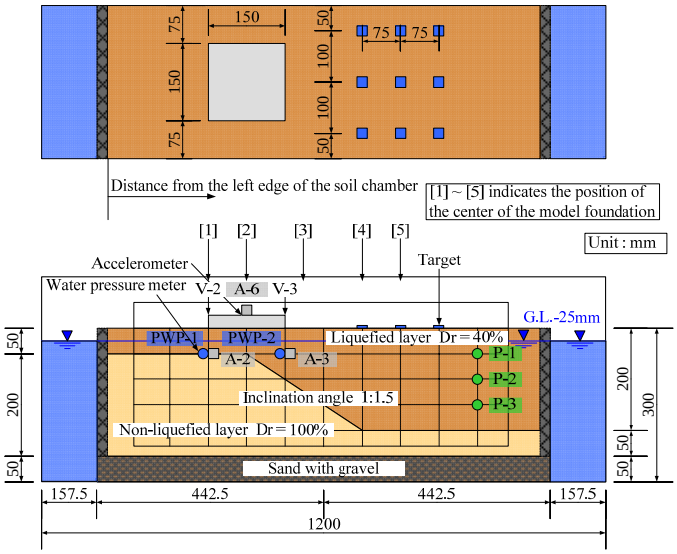

Figure 3.5. Sectional side view of model tests and the position of the center of the model foundation

Table 3.6. Shaking table model test cases

Case Name	Relative density Dr [%]	Distance from the left edge of the soil chamber [mm]	Thickness of liquefied layer [mm]	
			Left side	Right side
A-1 (position [1])	31.1	217.5	50	50
A-2 (position [2])	37.7	292.5	50	100
A-3 (position [3])	41.2	405.0	75	175
A-4 (position [4])	37.2	517.5	150	200
A-5 (position [5])	42.0	592.5	200	200

3.3. Results and discussion

Figure 3.6 shows time histories of the acceleration response, total settlement and differential settlement and the excess pore water pressure ratio for Case A-2, in which the liquefied layer under the model was unbalanced at both edges to represent the conditions of the houses in Zone A of Figure 2.1. Settlement of the model foundation occurred with an excess pore water pressure ratio (defined as the

ratio of excess pore water pressure to initial effective stress) of P-1 and P-2 reaching approximately 1.0. A significant difference in this ratio between PWP-1 and PWP-2 can be seen at the time of settlement. This appears to depend on the boundary condition between the liquefied and non-liquefied layers because no difference in acceleration response between A-2 and A-3 before the time of settlement is observed. Differential settlement arises due to differences in excess pore water pressure, and the phenomenon in Case A-2 can be attributed to such a difference between PWP-1 and PWP-2.

Table 3.7 and Figure 3.7 show the results of all cases for total/differential settlement, acceleration response and the excess pore water pressure ratio. These outcomes show that the differential settlement observed around the location where the thickness of the liquefaction layer varied drastically was the greatest among all the cases. Conversely, differential settlement at the location where the thickness of the liquefaction layer was uniform was smaller than in the other cases, although the total settlement was greater. The mechanism behind this phenomenon can be explained by the difference in acceleration response and the difference in pore water pressure between the right and left edges of the foundation. This means that the acceleration response tended to become amplified by reflection from the sloping non-liquefied layer, and that a difference in pore water pressure between the right and left edges of the foundation arose due to the constraint conditions seen near the non-liquefied layer.

4. CONCLUSIONS

In order to evaluate the relationships linking sloping geological structure, the thickness of the liquefaction layer and total/differential settlement of houses, shaking table model tests were performed. The following observations were made:

1. The response acceleration measured on the ground surface in the case with a thin liquefaction layer tended to be amplified regardless of liquefaction conditions. In contrast, the response acceleration observed on the ground surface in the case with a thick liquefaction layer tended to decay over time due to liquefaction.
2. The differential settlement observed around the location where the thickness of the liquefaction layer varied drastically was the greatest among all the cases. Conversely, differential settlement in the location where the thickness of the liquefaction layer was uniform was smaller than in the other cases.
3. The above conclusions based on the test results conform to those drawn from field investigation outcomes.

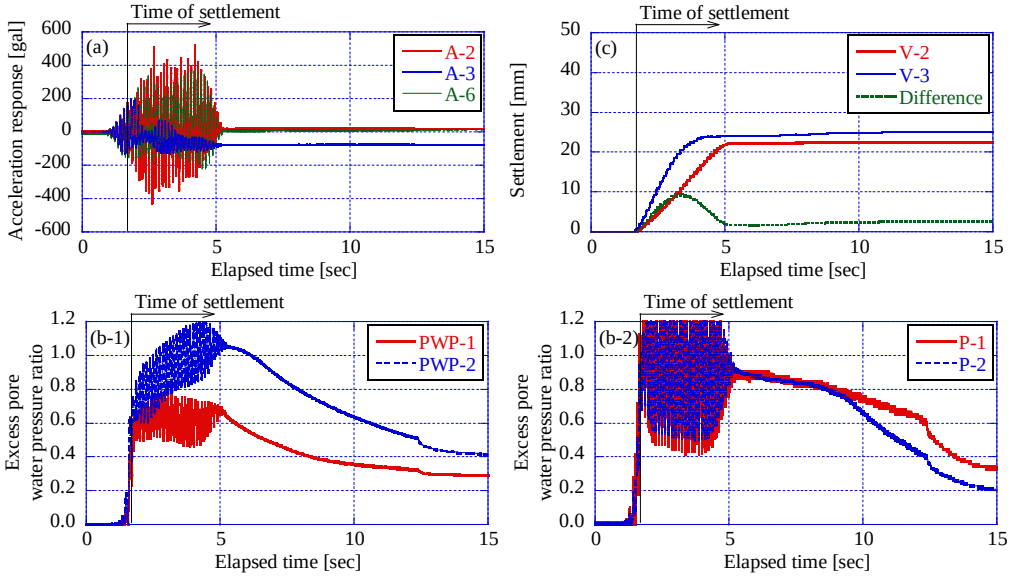

Figure 3.6. Time history of (a) acceleration response, (b) excess pore water pressure ratio and (c) total and differential settlement of Case A-2 in which the model foundation is located on the position [2]

Table 3.7. Settlement and differential settlement of each case

Test code	Relative density Dr [%]	Maximum acceleration of input wave [gal]	Ground water level [mm]	Settlement [mm]		Differential settlement [mm]
				Left side	Right side	
A-1 (position [1])	31.1	226.2	30.2	12.3	13.6	1.35
A-2 (position [2])	37.7	259.9	32.0	18.0	24.5	6.54
A-3 (position [3])	41.2	253.0	29.0	27.3	24.5	2.80
A-4 (position [4])	37.2	261.9	29.0	25.6	24.1	1.55
A-5 (position [5])	42.0	256.9	32.2	23.3	23.9	0.58

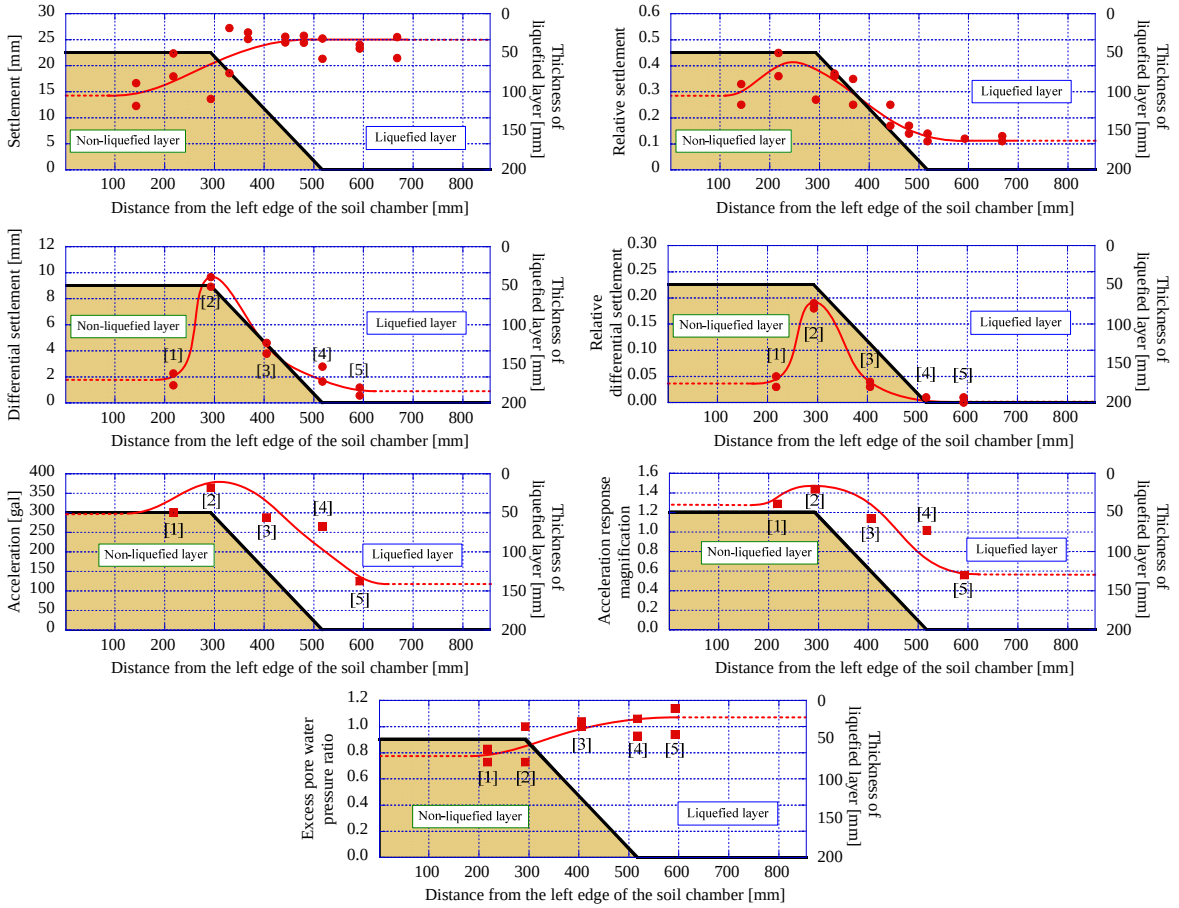

Figure 3.7. Comparison of (a) total settlement, (b) relative ratio of total settlement with respect to thickness of liquefied layer, (c) differential settlement, (d) relative ratio of differential settlement with respect to thickness of liquefied layer, (e) acceleration response, (f) acceleration response magnification and (g) excess pore water pressure ratio for all cases

REFERENCES

Andrus, R. D., Stokoe, K. H., and Chung, R. M. (1999). Draft guidelines for evaluating liquefaction resistance using shear-wave velocity measurements and simplified procedure, NISTIR6277, National Institute of Standards and Technology, Gaithersburg, Md.

Architectural Institute of Japan. (2008). Recommendations for the Design of Small Building Foundations, AIJ, Japan.

The Japanese Geotechnical Society. (2004). Investigation reports on the Niigata-ken Chuetsu Earthquake of 2004 (in Japanese), JGS, Japan.

Japan Road Association. (2002). Design Specifications for Highway Bridges: Part V: Seismic Design.

The Japanese Geotechnical Society. (2007). Investigation reports on the Niigata-ken Chuetsu-Oki Earthquake of 2007 (in Japanese), JGS, Japan.